Pergamon

Int. J. Heat Mass Transfer. Vol. 40, No. 14, pp. 3449–3465, 1997

Printed in Great Britain
0017–9310/97 $17.00+0.00

PII: S0017-9310(96)00376-6

Oscillatory natural convection of water near the density extremum at high Rayleigh numbers

T. NISHIMURA, Y. HAYASHIDA and M. MINEOKA

Department of Mechanical Engineering, Yamaguchi University, Ube 755, Japan

and

A. WAKE

Shimizu Corporation, Tokyo 135, Japan

(*Received* 19 *October* 1995 *and in final form* 2 *August* 1996)

Abstract—An experimental investigation has been conducted with regard to the natural convection of water near the density extremum in rectangular enclosures with the vertical walls held at different temperatures. The water in the enclosure is initially set at a uniform temperature and then the temperatures of the cold and hot walls are suddenly changed to 0 and 8°C, respectively. The flow patterns of the steady state are presented for the initial temperature range of 2–6°C at high Rayleigh numbers, not considered previously. At an initial temperature of 4°C, the convective flow field consists of a symmetric double-cell circulation forming a downward flow, called a sinking jet in the interior of the enclosure. For $Ra > 9 \times 10^6$, the interior sinking jet shows an oscillatory behavior due to free-shear instability, which enhances the heat transfer rate between vertical walls. However, at an initial temperature other than 4°C, an asymmetric double-cell circulation is revealed. Oscillatory flow is suppressed near the vertical walls. These phenomena are satisfactorily explained by a numerical analysis. © 1997 Elsevier Science Ltd.

INTRODUCTION

Many natural phenomena involve buoyancy-induced flows of cold water close to the freezing point. The mechanism of such flows is complicated considerably by the fact that its density reaches maximum value at about 4°C, giving rise to a variety of intriguing results. Many experimental and numerical studies of natural convection concerned with the effect of the density inversion of water have been carried out in enclosures with vertical hot and cold walls at Rayleigh numbers less than 10^6 [1–8]. The numerical solutions satisfactorily predicted the experimental results, indicating that the density inversion of water has a great influence on natural convection.

Furthermore, there have been a few studies related to natural convection at high Rayleigh numbers ($Ra > 10^6$), which is associated with the issues of energy and ecology. Lankford and Bejan [9] conducted experiments in a high-aspect ratio enclosure ($A = 5.05$) where a constant heat flux boundary condition was imposed on the hot vertical wall, while the opposite wall was cooled to temperatures below 4°C. A scale analysis was used to correlate the average Nusselt number measured experimentally in the Rayleigh number range of 10^8 to 10^{11}. Ivey and Hamblin [10] performed experiments of natural convection in low-aspect ratio enclosures ($A = 0.059$–0.265) filled with water at high Rayleigh numbers ($Ra = 10^5$–10^8). The vertical hot wall temperature was 8°C and the cold wall temperature was 0°C. The flow field consisted of a double-cellular circulation, but the flow was not always stable; that is, downward flow called a sinking jet was observed at the central portion of the enclosure showing large-scale meanders for $Ra > 10^7$. An apparently similar feature was reported by Lankford and Bejan [9]. Braga and Viskanta [11] investigated experimentally and numerically the transient natural convection in a rectangular enclosure ($A = 0.5$) in the Rayleigh number range of 10^7–10^8. The fluid was initially stagnant at 8°C, then the temperature of one vertical wall was suddenly lowered to 0°C. The authors' attention was focused on flow development in the presence of a density inversion. McDonough and Faghri [12] performed similar experiments and numerical analysis of the transient and steady-state natural convection of water in a rectangular enclosure ($A = 0.75$) by varying the initial and hot wall temperatures at $Ra = 10^7$, and the experimental results agreed with numerical steady-state solutions. They observed an asymmetric convective flow pattern under conditions where the hot- and cold-wall temperatures were kept at 8 and 0°C, respectively, and the initial temperature is 8°C instead of 4°C.

Experimental studies, therefore, suggested that flow in the presence of density inversion becomes oscillatory at high Rayleigh numbers. However, the inception of flow instability and its subsequent effect on

NOMENCLATURE

A	aspect ratio ($=H/L$)
d_c	critical depth for unstable flow measured from the top of the enclosure
g	gravitational acceleration
H	height of the enclosure
L	horizontal length of the enclosure
Nu_z	local Nusselt number
Ra	Rayleigh number defined by equation (2)
T	temperature
T_b	bulk temperature
T_c	temperature at the cold wall ($=0°C$)
T_h	temperature at the hot wall ($=8°C$)
T_i	initial temperature
T^*	reference temperature ($=4°C$)
t	time
W	depth of the enclosure ($=17$ cm)
x	horizontal coordinate
z	vertical coordinate.

Greek symbols

α^*	reference thermal diffusivity
ν^*	reference kinematic viscosity of fluid
η_m	distance from the cold wall to the position of sinking jet flow at mid-height
ρ	density of fluid
ρ^*	reference density of fluid of 4°C.

heat transfer have not been studied in detail. These facts motivated a previous study [13] in which numerical calculations of natural convection were performed with the density inversion of water in a rectangular enclosure with $A = 1.25$, in the Rayleigh number range of 10^5–10^8. The numerical analysis provided steady-state solutions even at high Rayleigh numbers, contrary to expectations based on previous experiments by other investigators. Therefore, the present experiment was performed to examine the onset of oscillatory flow and the main features of the flow, comparing the authors' previous numerical investigation. We also examined the effect of the initial temperature on the flow pattern, because Braga and Viskanta [11] and McDonough and Faghri [12] suggested the significance of the initial temperature. Thus, two experiments were conducted, with initial temperatures of $T_i = 4°C$ for Case 1 and T_i other than 4°C for Case 2.

EXPERIMENTS

The experiments were performed in enclosures of three different sizes which were the same as those in the previous numerical study [13]. The geometric aspect ratio and the depth of the enclosures were fixed ($A = 1.25$ and $W = 17$ cm). The height H and horizontal length L of the enclosures were 15×12 cm, 20×16 cm and 40×32 cm corresponding to Rayleigh numbers $Ra = 1.68 \times 10^7$, 4×10^7 and 3.2×10^8, respectively. Figure 1 illustrates a schematic of the experimental apparatus. The main parts of the apparatus are for cooling, testing, and heating. The test section was a rectangular enclosure consisting of an acrylic resin frame (15 mm thick) placed between two copper plates (5 mm thick), corresponding to the hot and cold walls. Several thermocouples were imbedded in the hot and cold walls for continuous temperature monitoring. Each wall was attached to a heat exchanger connected to three loops through which the flow rate of coolant could be controlled independently. The heat exchangers were connected through a valve system on each constant-temperature bath. Methyl alcohol was used as the coolant in these baths. In order to minimize heat loss, the experimental apparatus was covered with styrofoam insulating material 60 mm thick and, in addition, the apparatus was placed in a cold room with temperature controller. Two removable windows in the insulation allowed for illumination and visual observation.

Measurements of the bulk temperature in the enclosure were made with copper–constantan thermocouples of 100 μm in diameter. They were placed in a plastic tube with an o.d. of 2 mm. These probes were inserted through 10 holes located in the back wall of the enclosure, as shown in the figure. The uncertainty in temperatures includes the error within 0.1°C.

Distilled water was used in all experiments and the water was carefully siphoned into the enclosure to avoid introduction of air. Before the start of each experiment, both heat exchangers were coupled to the baths with the same constant temperature and the hot and cold walls were maintained at the desired initial temperature T_i. After sufficient time for the water in the enclosure to reach the uniform temperature, a test run was started by simultaneously changing the temperatures of coolants in the two heat exchangers. In practice, it took about 15–20 min for the cold and hot walls of the largest enclosure to reach the desired temperatures of $T_c = 0°C$ and $T_h = 8°C$.

In the previous experimental studies [9, 10, 12], the flow field of natural convection with density inversion was visualized by a dye injection method or a thymol blue pH indicator technique. It is important to understand the connection between flow and temperature fields for time-dependent natural convection, such as oscillatory flow. However, these techniques do not

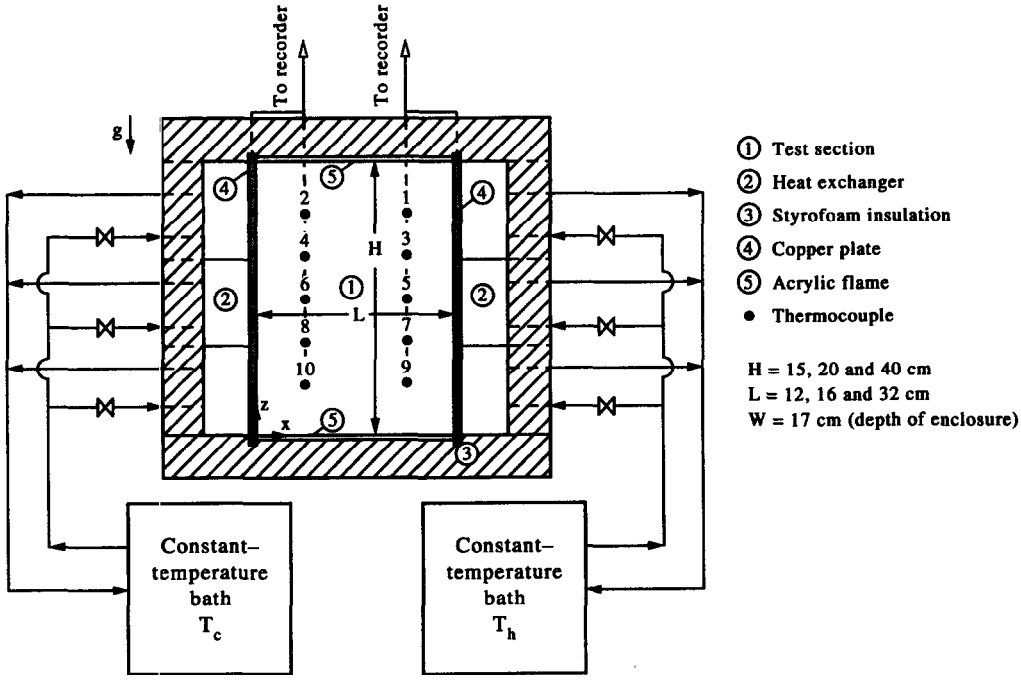

Fig. 1. Schematic diagram of experimental apparatus.

provide this connection. Therefore, an alternative technique, i.e. the thermosensitive liquid crystal tracer method was used. This method has been verified as being helpful in interpreting time-dependent natural convection. For example, Nishimura *et al.* [14, 15] used liquid crystal particles to examine the flow and temperature fields of double-diffusive convection.

The liquid crystals used here were microcapsulated particles manufactured by BDH Chemicals, Ltd, and were chosen to cover a temperature range of 2.5–5°C in order to focus on density inversion of water. The colors change from red at the lowest temperature, through yellow and green, to blue at the highest one. The density of encapsulated liquid crystals was about 1.02×10^3 kg/m^3 and their diameter ranged from 10 to 15 μm. The volume of liquid crystals suspended in the distilled water was 0.002 vol%. We preliminarily examined the effect of the presence of liquid crystals on the flow and temperature fields for three enclosures and confirmed a negligible effect on thermal stratification in the bulk fluid and temperature oscillations. The time constant for the temperature variation of the liquid crystals is about 0.3 s; therefore, the delay in their response to the temperature range was short for the flow field in the present study. Light was introduced through a slit by a 300 W projector lamp.

NUMERICAL ANALYSIS

The numerical method used here is the same as that in the previous study [13]. Only the relevant definitions and assumptions are described here. The water has a nonlinear density–temperature relationship that attains its maximum at a temperature of about 4°C. Several investigators have proposed different correlations for the density of water as a function of temperature. The present study utilizes a parabolic form of the correlation over the range 0–8°C, as suggested by Simons, [16]:

$$\rho = \rho^*[1 - B^*(T - T^*)^2] \tag{1}$$

where $B^* = 6.8 \times 10^{-6}$ (°C)$^{-2}$, T^* is the reference temperature of 4°C and ρ^* is the reference density of 4°C. The definition of the Rayleigh number is

$$Ra = g\Delta\rho H^3/(\rho^* \nu^* \alpha^*) = gB^*(T^* - T_c)H^3/(\nu^* \alpha^*) \tag{2}$$

where thermophysical properties are evaluated at the reference temperature.

It should be noted that in this system, the Rayleigh number varies only with the enclosure height H, because the temperatures at the vertical walls are fixed, i.e. 0 and 8°C.

Initially ($t < 0$), the water in the enclosure was stagnant at a uniform temperature, T_i. When $t > 0$, the opposing vertical walls of the enclosure were cooled to 0°C and heated to 8°C, respectively. The following assumptions have been made in the analysis: (1) the flow is two-dimensional and incompressible; (2) the thermophysical properties are independent of temperature, except for the density in the buoyancy force; (3) the top and bottom connecting walls are insulated. These simplifications have been often employed in previous studies [11, 12] to reduce the computational effort.

The governing equations expressed in terms of the velocities and the pressure have been solved numeri-

cally using a penalty finite element method. The characteristics of the algorithm used here are summarized as follows: (1) four-noded bilinear isoparametric elements are used for spatial discretization; (2) the Crank–Nicolson method is used for discretization of the time derivative terms; (3) convective and buoyancy force terms are treated explicitly in time while other terms remain implicit. This method has a significant advantage in computational efficiency since the pressure can be eliminated from the unknowns.

RESULTS AND DISCUSSION

Case 1 : $T_i = 4°C$

First, we present the results for the largest enclosure ($H \times L = 40 \times 32$ cm corresponding to $Ra = 3.2 \times 10^8$). Figure 2 shows the time variation of temperatures in the core region. The position of thermocouples is also denoted in the figure. In response to the heating and cooling of the vertical walls, the temperatures (nos 1, 3, 5 and 7, $T > 4°C$) increase at the hot wall side, while the temperatures (nos 2, 4, 6 and 8, $T < 4°C$) decrease at the cold wall side. However, after 65 min from the start of the experiment, the temperatures of nos 3, 5 and 7 at the hot wall side decrease and then reach a steady-state. Similar reverse-patterns are observed at the cold wall side (see temperatures of nos 4 and 6). This appears to be due to the horizontal mixing of fluid caused by the onset of oscillatory flow, which is suggested by the fluctuation in the temperatures of nos 6, 8 and 10 observed at about 40 min.

Figure 3 shows the corresponding visualization photographs by liquid crystals after 180 min from the beginning of the experiment. An exposure time of 2 s was used. Figure 3(a) shows the flow and temperature fields near the cold wall for reference purposes, since a similar pattern is observed near the hot wall. Low-density fluid rises along the cold wall and a thermal boundary layer is observed clearly from the isotherms indicated by liquid crystals. The upward flow is two-dimensional and stable, the maximum vertical velocity at mid-height is evaluated $0.34\alpha^* Ra^{1/2}/H$ by the particle paths of liquid crystals and its value is close to the solution of boundary layer theory [13]. Thus, at $Ra = 3.2 \times 10^8$, there is no wall boundary layer instability like Tollmien–Schlichting waves which are observed for water without density inversion in a square cavity at about $Ra = 10^{10}$ [17]. The flow and temperature visualizations near the top of the enclosure are shown in Fig. 3(b). The opposing thermal intrusion layers, emanating from each vertical wall, meet near the centre of the top, turn and sink toward the bottom. The flow maintained is still two-dimensional and stable. Here we call the downward flow a sinking jet, since the nature of flow is similar to a planar jet as indicated by previous numerical study [13]. The maximum velocity of the sinking jet corresponds to the isotherm of 4°C. Figure 3(c) shows the flow and temperature fields in the core region. The sinking jet becomes unstable beyond a critical depth measured from the top of the enclosure ($d_c = 0.15H$) and largely meanders in x-direction. Therefore, after the fluid whose temperature is less than 4°C mixes with the fluid of more than 4°C, the bulk fluid is maintained near 4°C in the lower part of the enclosure. The behavior of fluid mixing is made discernible by the colors of the liquid crystals, with green approximately indicating the 4°C isotherm. Two-dimensional flow is maintained slightly downstream from the critical depth, but further downstream the flow becomes three-dimensional, in contrast to the boundary layer which flows along the vertical walls. This sinking jet divides into two oppositely directed flows along the bottom toward the base of respective vertical walls. Thus, it can be inferred that the oscillatory sinking jet is self-imposed, i.e. the free-shear instability of the sinking jet rather than the wall boundary layer instability.

The unstable flow was also observed for the two smaller enclosures with the same aspect ratio ($H \times L = 15 \times 12$ cm and 20×16 cm corresponding to $Ra = 1.68 \times 10^7$ and 4×10^7). The critical depth for the onset of unstable flow was also determined by the flow visualization. Figure 4 shows the relationship between the critical depth and the Rayleigh number for $A = 1.25$. A linear relationship on a log–log plot is obtained in the Rayleigh number range considered here. The solid line denotes the boundary between unstable and stable flows. The experimental result by Ivey and Hamblin [10] is also shown ($Ra = 4 \times 10^7$ and $A = 0.4$) in the figure and lies on the solid line. If this relationship holds good even at lower Rayleigh numbers, we can estimate the onset of unstable flow, i.e. $Ra = 9 \times 10^6$ for $d_c/H = 1.0$. This critical value, with $A = 1.25$, is almost equal to that in the experiments, with $A = 0.324$–0.53, by Ivey and Hamblin. The effect of geometric aspect ratio seems to be small at high Rayleigh numbers except for high aspect ratios.

Figure 5 shows temperature fluctuations representing oscillatory flow, which have not been measured previously. Figure 5(a) shows the results at $x/L = 0.6$ and $z/H = 0.7$ for $Ra = 3.2 \times 10^8$. The position is marked by a cross symbol in Fig. 3(c). After 1000 s from the beginning of the experiment, the temperature increases above 4°C because the measuring point is located at the hot wall side. However, after 5400 s the temperature falls intermittently below 4°C, indicating the onset of oscillatory flow and then periodic oscillation is maintained. The signal is not sinusoidal, but spiky, suggesting the onset of turbulence. The peak-to-valley amplitude and period of temperature oscillation were approximately 2°C and 250 s, respectively. Figure 5(b) shows the results at $x/L = 0.55$ and $z/H = 0.4$ for $Ra = 4 \times 10^7$. Although a periodic oscillation in temperature is observed after intermittent fluctuations, the signal is sinusoidal rather than spiky. The period of oscillation is about

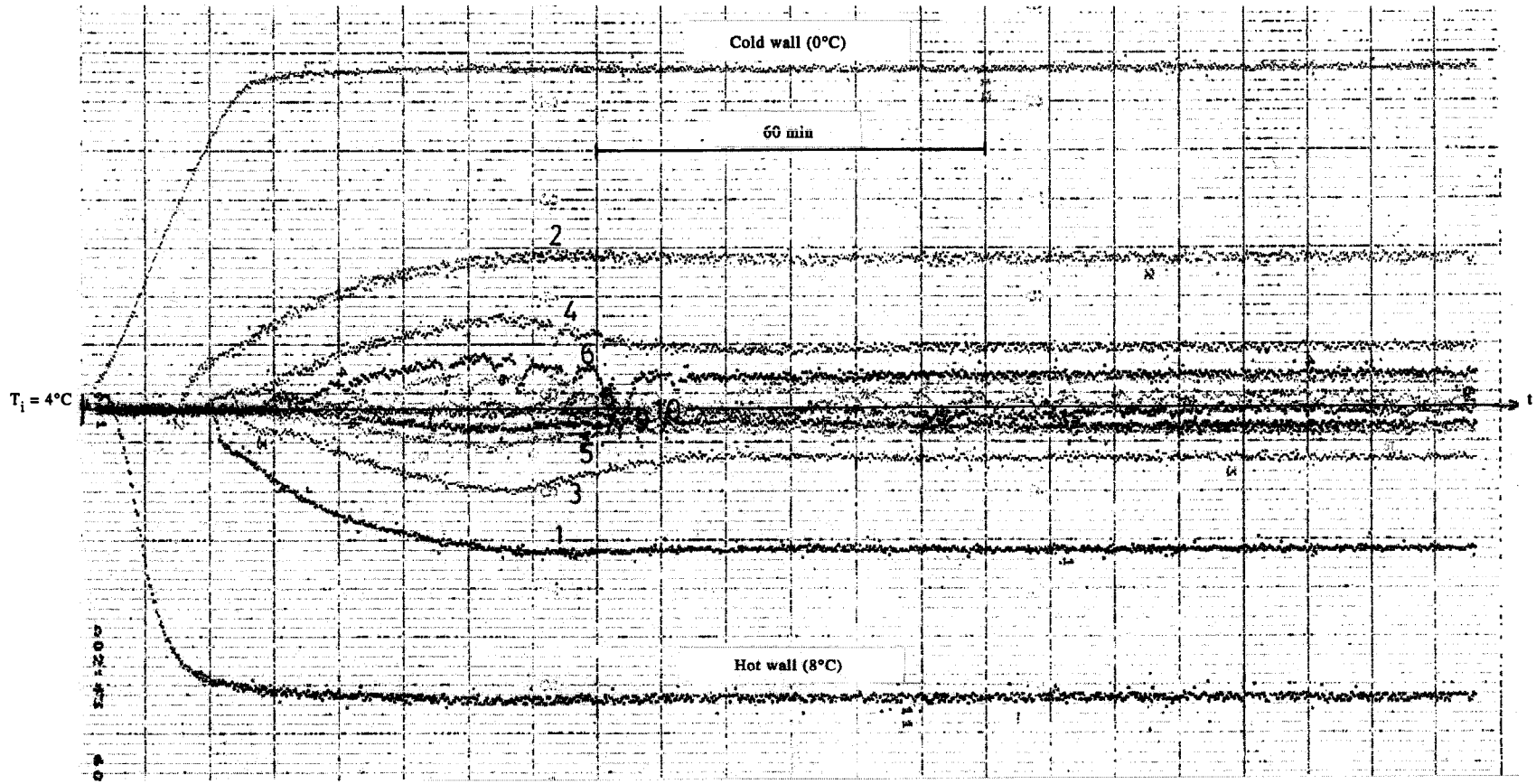

No.	1	2	3	4	5	6	7	8	9	10
x/L	0.75	0.25	0.75	0.25	0.75	0.25	0.75	0.25	0.75	0.25
z/H	0.85	0.85	0.68	0.68	0.5	0.5	0.32	0.32	0.15	0.15

Fig. 2. Time variation of temperatures in the core region for $T_i = 4°C$ at $Ra = 3.2 \times 10^8$ corresponding to a 40×32 cm enclosure.

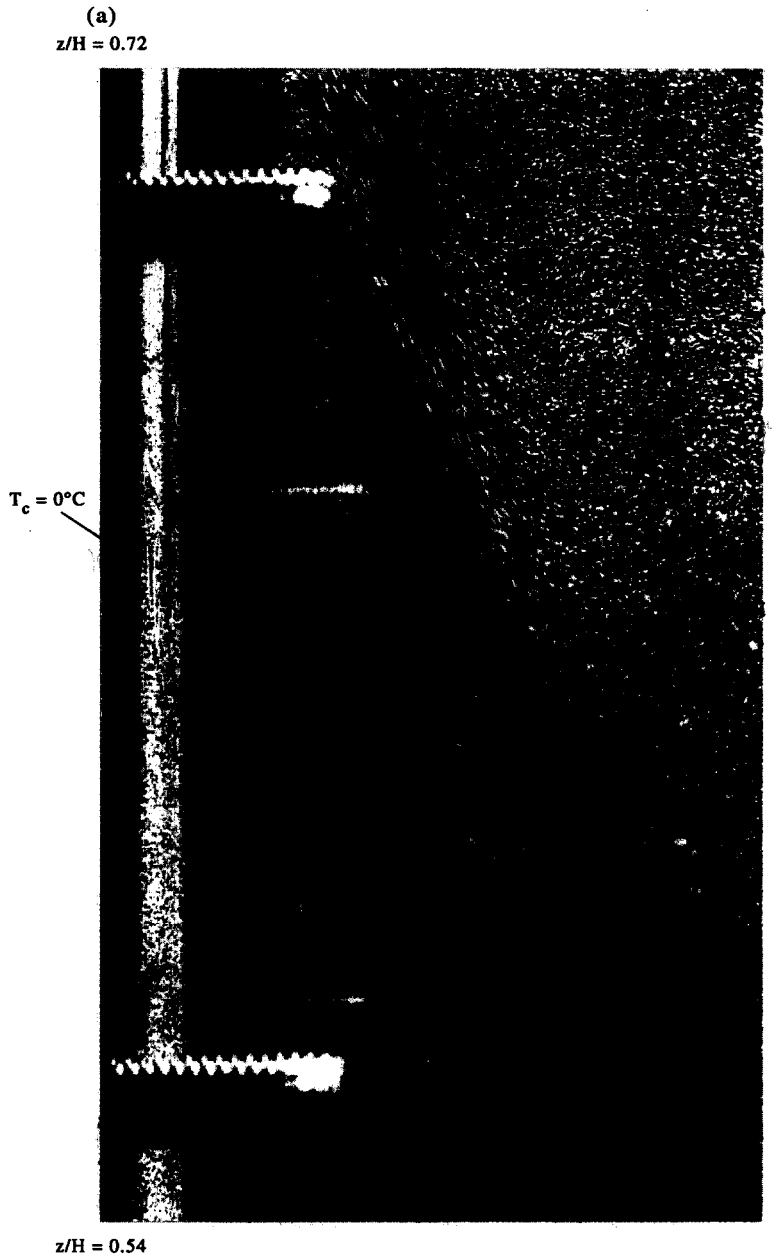

Fig. 3. Visualization photographs of temperature and flow fields at $Ra = 3.2 \times 10^8$ by liquid crystals: (a) cold-wall region; (b) top-wall region; and (c) core region. (*Continued opposite and overleaf.*)

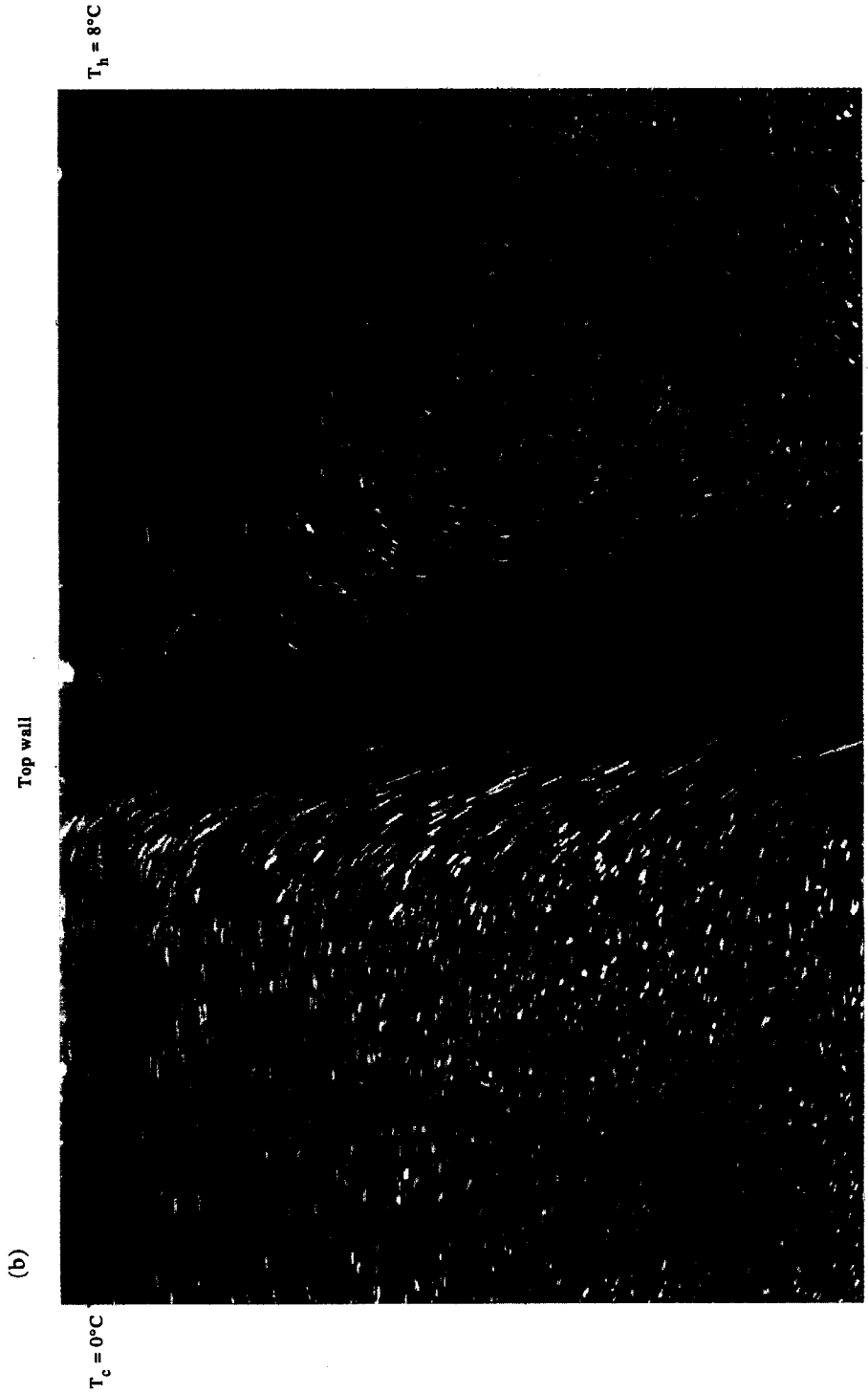

Fig. 3—*continued.*

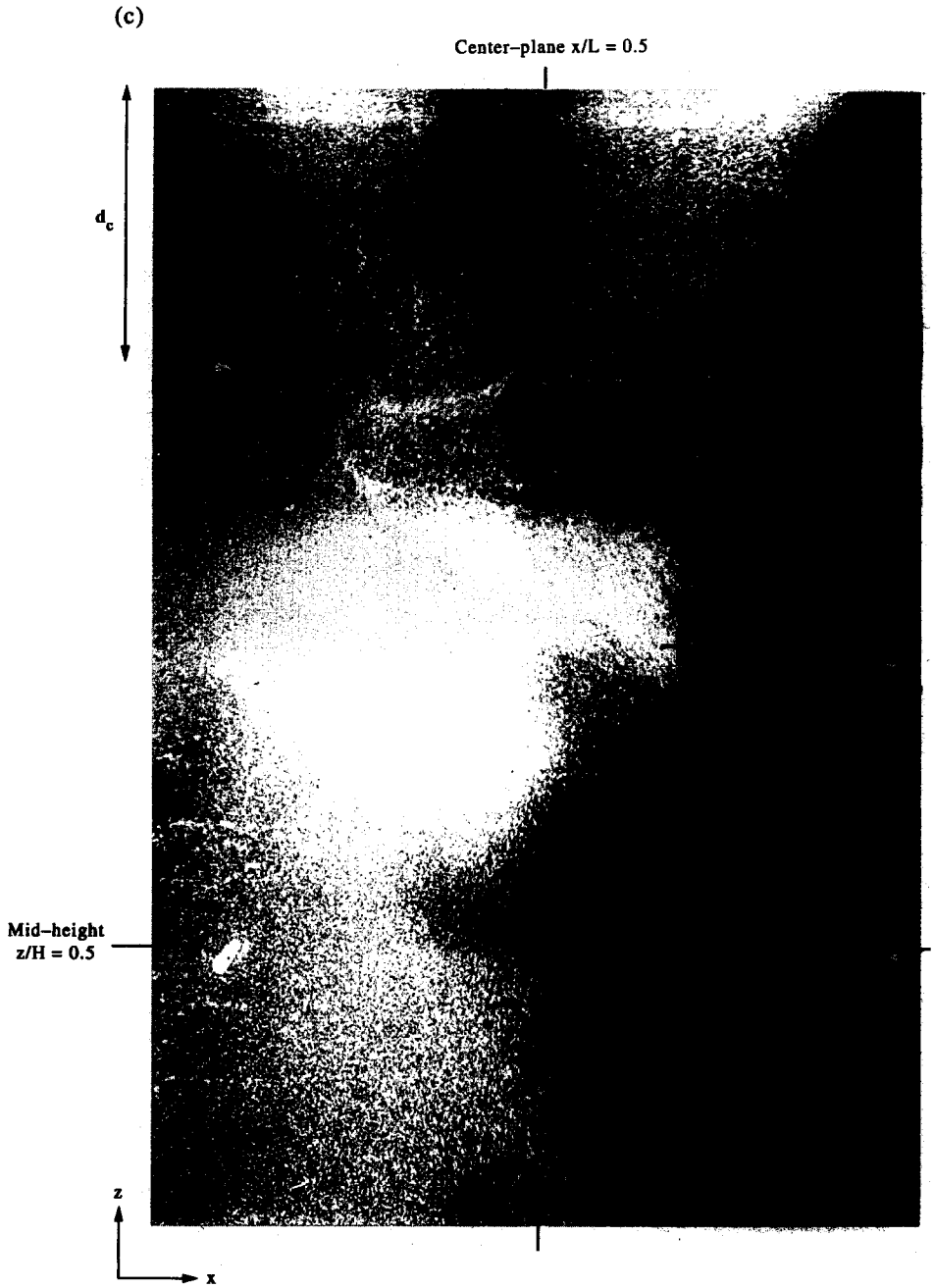

Fig. 3—*continued.*

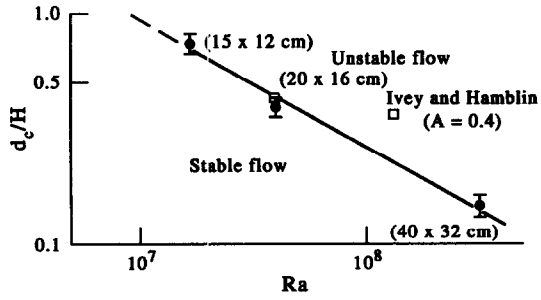

Fig. 4. Critical depth for the onset of unstable flow vs Rayleigh number for $A = 1.25$.

290 s and almost equal to that for $Ra = 3.2 \times 10^8$. A similar result obtained near the bottom of the enclosure for $Ra = 1.68 \times 10^7$ is not shown here.

Figure 6 shows the thermal stratifications at $x/L = 0.25$ and 0.75 in the core region for three Rayleigh numbers at 180 min. The filled symbol denotes $x/L = 0.25$ in the cold-wall side and the open symbol is $x/L = 0.75$ in the hot-wall side. Each experiment was repeated four times and the temperatures were averaged. Uncertainties have been denoted by error bars in the figure. The dotted lines represent the steady-state numerical solution in the previous study [13] and are independent of Rayleigh number in the boundary layer flow regime ($8.25 \times 10^5 < Ra < 3.2 \times 10^8$). The solid lines denote the oscillatory-state numerical solution at $Ra = 3.2 \times 10^8$, which has been obtained in the present study. The experimental data at $Ra = 1.68 \times 10^7$ are almost on the dotted lines, although slightly scattered, because the unstable region below the critical depth is limited near the bottom of the enclosure, as marked in the ordinate of the figure. However, as the Rayleigh number increases to 4×10^7, the experimental data deviate from the dotted lines. The difference is significant in the lower part of the enclosure, where the temperatures are close to 4°C. This is because the critical depth becomes smaller with an increase of Rayleigh number and the horizontal fluid mixing is enhanced in the core region, as observed in the flow visualization photograph of Fig. 3(c). A comparison between the solid lines and the experimental data for $Ra = 3.2 \times 10^8$ is explained later in this paper.

The above experiments confirm the onset of oscillatory flow at high Rayleigh numbers, contrary to steady flow based on the previous numerical study [13], leading to the conclusion that modification of the numerical model is needed.

For oscillatory flow, the flow pattern is asymmetric at about the midpoint of the enclosure, as shown in Fig. 3(c). In the previous numerical study, a symmetric flow pattern was observed throughout the transient and steady states. Asymmetries of temperature and velocity may be needed for the flow to become unstable and oscillatory. These can be obtained numerically by considering an offset from the initial temperature of 4°C, the variable thermophysical properties such as the kinematic viscosity and thermal diffusivity of water, or by using an asymmetric density–temperature relationship as proposed by other investigators. In the present study, a slight offset from

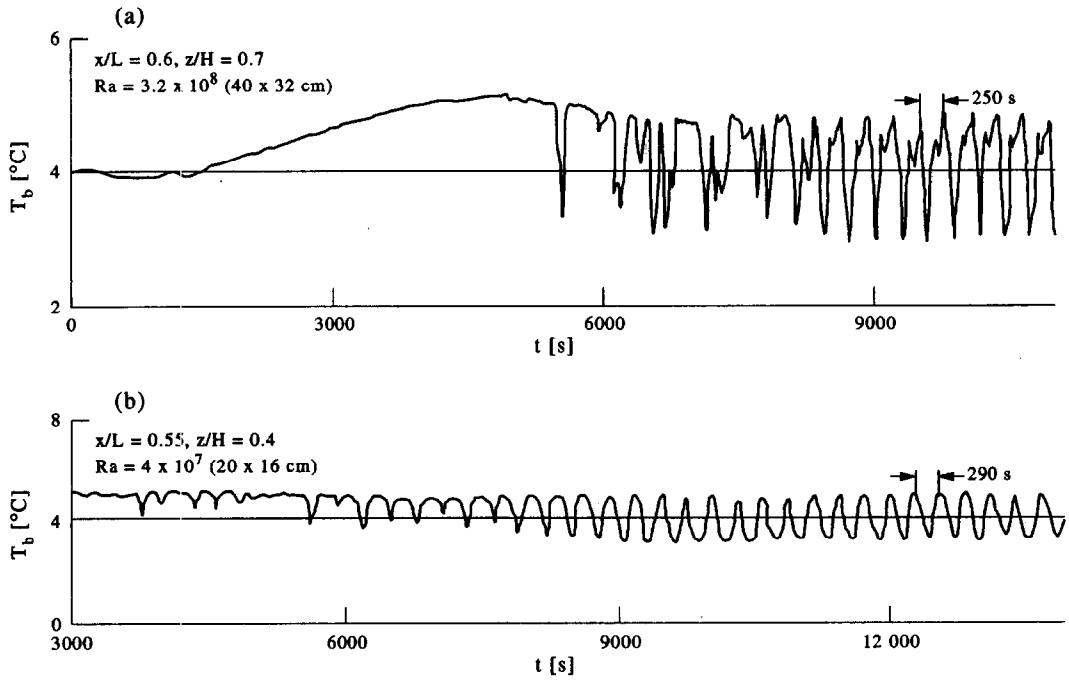

Fig. 5. Time history of temperature representing self-sustained oscillation at $Ra = 3.2 \times 10^8$ and 4×10^7.

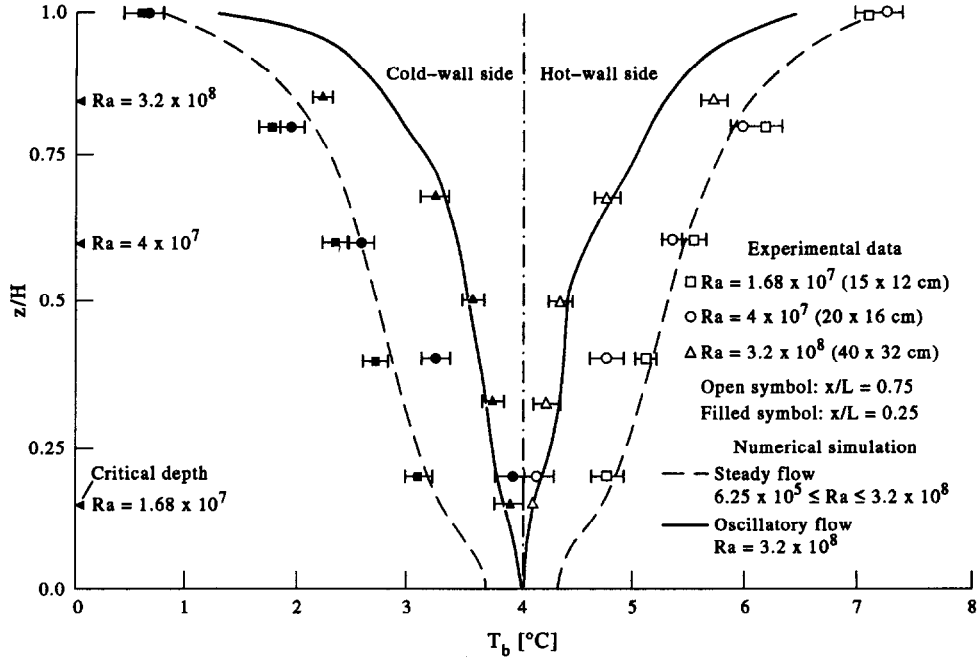

Fig. 6. Thermal stratification in the core regions for different Rayleigh numbers.

the initial temperature of 4°C was considered as an initial step. The initial temperature is assumed to be 4.1°C, in the view of the uncertainty about the initial temperature in the experiments. The computation is performed for the largest enclosure ($H \times L = 40 \times 32$ cm corresponding to $Ra = 3.2 \times 10^8$), assuming two-dimensional flow. The numerical procedure is the same as that in the previous study [13] and a non-uniform mesh with 60×62 nodal points was used. The solution agreed with that with 48×52 nodal points in terms of the period of oscillation and local Nusselt numbers within 3%.

Figure 7 shows the sequence of transient streamlines for different times. The flow is asymmetric and the size of circulation at the right hot wall is slightly larger than that at the left cold wall. Because the isotherm of 4°C slightly moves from the enclosure center to the cold wall side for $T_i = 4.1$°C. After a strong sinking jet is formed in the interior of the enclosure ($t = 1800$ s), several vortices are observed in the region of the sinking jet as a result of a free-shear instability, which maintains self-sustained oscillation. However, respective boundary layer flows along the vertical walls are stable. Therefore, the predicted main features of the sinking jet and boundary layer flows are similar to the experimental results.

Figure 8 shows fluctuations of the horizontal velocity and temperature at $x/L = 0.46$ and $z/H = 0.623$. The velocity oscillates between positive and negative values, indicating horizontal fluid mixing, where a positive value indicates the flow from the hot wall to the cold wall. The temperature fluctuation follows the velocity one with a slight phase lag. The period of oscillation in the temperature averages 310 s, which is 20% larger than the experimental value shown in Fig. 5(a).

The comparison of numerical and experimental thermal stratification in the core region is also illustrated in Fig. 6. The solid lines denote time-averaged temperatures of the present numerical solutions during one oscillation cycle. The agreement with the experimental data for $Ra = 3.2 \times 10^8$ is satisfactory except near the top of the enclosure, where the experimental data reach the dotted lines rather than the solid lines. This is because the experimental critical depth for the onset of unstable flow is larger than the numerical one.

Although there is partial agreement between experimental and numerical results, the disagreement claims that further consideration of the numerical model is subject of a future work, e.g. the effects of variable thermal properties, asymmetric density–temperature relationship and three-dimensional flow not considered in the present study.

The horizontal fluid mixing due to the oscillatory sinking jet probably enhances the heat transfer rate between the hot and cold walls. Because the temperature difference between each vertical wall and the corresponding core region becomes larger for oscillatory flow than steady flow as shown in Fig. 6. Figure 9 shows the predicted local Nusselt numbers along the cold wall for steady and oscillatory flows. The Nusselt number for oscillatory flow is an instantaneous value at $t = 7770$ s. It is noted that although the sinking jet

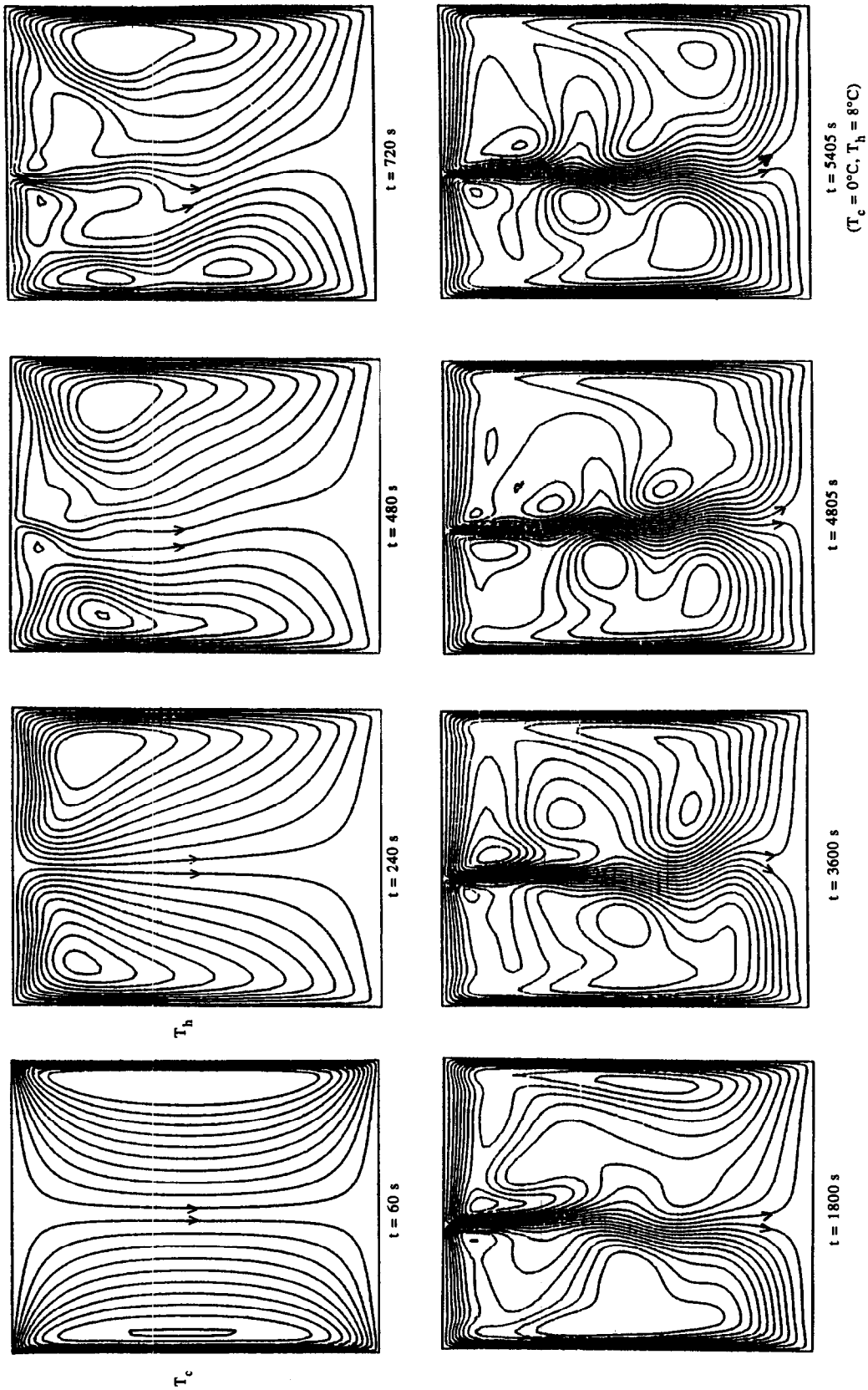

Fig. 7. Numerical streamlines at different times for oscillatory-state at $Ra = 3.2 \times 10^8$.

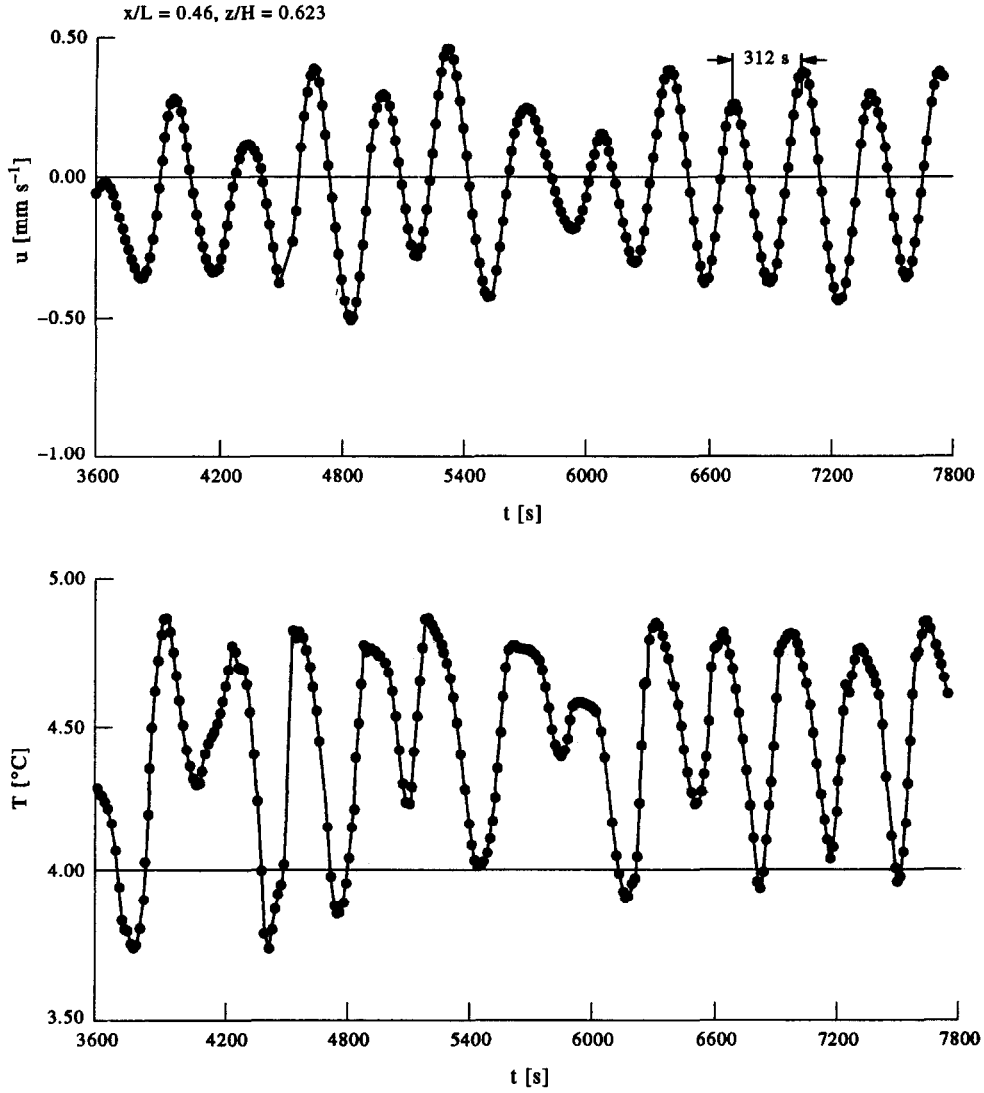

Fig. 8. Time variation of numerical velocity and temperature at $Ra = 3.2 \times 10^8$.

oscillates significantly, the Nusselt number fluctuation at the cold wall is less than 1%, as expected from the streamline patterns shown in Fig. 4. Since the thermal boundary layer develops stably from the base of the cold wall, the local Nusselt number decreases in the vertical direction. The Nusselt number for oscillatory flow is found to be 20% larger than that for steady flow. Unfortunately, we could not obtain the experimental Nusselt number, because measurement of heat fluxes through the hot and cold walls is difficult in this experimental apparatus.

Case 2: T_i *other than* 4°C

The experimental and numerical studies by Braga and Viskanta [11] and McDonough and Faghri [12] discovered that the convective flow pattern becomes asymmetric for steady state when the initial temperature is 8°C, instead of 4°C, in an enclosure subjected to different temperatures ($T_c = 0$°C and $T_h = 8$°C), but the asymmetric flow was not examined in detail. The effect of initial temperature on the flow pattern for all three enclosures was, therefore, studied, providing further information on the sinking jet nature.

Figure 10 shows a representative visualization photograph at $T_i = 6$°C for an enclosure of $H \times L = 15 \times 12$ cm. The photograph represents the steady-state temperature and velocity field on the left-hand side of the enclosure, i.e. at the cold wall. The sinking jet is stably located near the cold wall, i.e. $\eta_m/L = 0.091$, where η_m is the distance from the cold wall to the position of sinking jet at mid-height of the

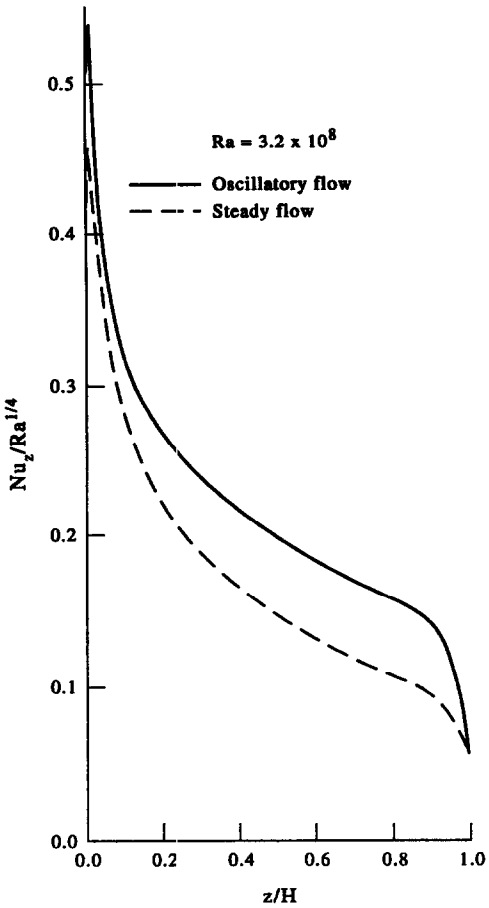

Fig. 9. Numerical local Nusselt number for steady and oscillatory flows at $Ra = 3.2 \times 10^8$.

enclosure. This is in sharp contrast with the result at $T_i = 4°C$. Figure 11 shows the steady-state numerical streamlines and isotherms for $T_i = 6°C$. They agree qualitatively with the flow visualization photograph shown in Fig. 10. Figure 12 shows the thermal stratification in the core region of a large circulation for two different initial temperatures ($T_i = 6$ and $2°C$). The solid line in the figure for $T_i = 6°C$ denotes the numerical solution at $x/L = 0.75$ satisfactorily agrees with the experimental data. The experimental thermal stratifications for $T_i = 6$ and $2°C$ are identical in the reverse situation and are close to the steady-state numerical solutions for $T_i = 4°C$ indicated by the dotted lines.

It is, therefore, recognized that the position of sinking jet shifts to the cold wall side for $T_i > 4°C$ and to the hot wall side for $T_i < 4°C$. The reason for this asymmetric flow is explained by the following example. If $T_i > 4°C$, the isotherm of $4°C$ with maximum density is located near the cold wall in the early stages of the experiment. After that, the thermal boundary layers along the hot and cold walls develop and the steady-state occurs under conditions where the heat fluxes are identical for both walls, while the flow pattern remains asymmetric. The inference is evident when the thickness of the steady-state cold thermal boundary layer is sufficiently smaller than the distance from the cold wall to the position of the sinking jet corresponding to the isotherm of $4°C$. Thus, the asymmetry is not observed at low Rayleigh numbers, but is realized at high Rayleigh numbers as suggested by McDonough and Faghri [12].

The asymmetric flow is also true of an enclosure of $H \times L = 20 \times 16$ cm at $T_i = 6°C$. The value of η_m/L is smaller than that for a 15×12 cm enclosure, i.e. 0.064, and the sinking jet is stable in contrast with the result for $T_i = 4°C$. This is probably because, for the sinking jet near the cold wall, the growth of free-shear instability is suppressed as compared with the sinking jet located in the interior of the enclosure. A similar pattern has been observed between a transitional wall jet and a free jet [18].

For the largest enclosure of $H \times L = 40 \times 32$ cm at $T_i = 2°C$, the sinking jet shifts to the hot wall side, but a steady state is not maintained, i.e. oscillatory flow, as shown in Fig. 13. A comparison between Figs. 3(a) and 13 indicates that the amplitude of oscillation at $T_i = 2°C$ is suppressed in the vicinity of the hot wall. Therefore, it should be noted that, at a higher Rayleigh number, the flow becomes unstable even if the sinking jet is located near the vertical walls.

CONCLUSIONS

In the present study, two experiments were conducted for three rectangular enclosures of $A = 1.25$, with initial temperatures of $T_i = 4°C$ for Case 1 and T_i other than $4°C$ for Case 2, in order to examine the effect of the density inversion of water at high Rayleigh numbers. The vertical walls of the enclosures were maintained at $T_c = 8°C$ and $T_h = 0°C$, respectively. The following conclusions have been drawn.

(1) For $T_i = 4°C$, the flow becomes unstable for $Ra > 9 \times 10^6$. The sinking jet in the interior of the enclosure maintains self-sustained oscillation due to free-shear instability, which leads to heat transfer enhancement.

(2) For T_i other than $4°C$, the sinking jet shifts toward the vertical walls of the enclosure and the flow becomes asymmetric, in contrast to Case 1. Therefore, the growth of instability is suppressed, and flow oscillations observed in Case 1 disappear in Case 2 under certain conditions.

Although these phenomena are satisfactorily explained by the two-dimensional numerical analysis, further consideration on the numerical model is needed for oscillatory flow, e.g. the effect of variable thermal properties, asymmetric density–temperature relationship and three-dimensional flow. This will be the subject of future investigation.

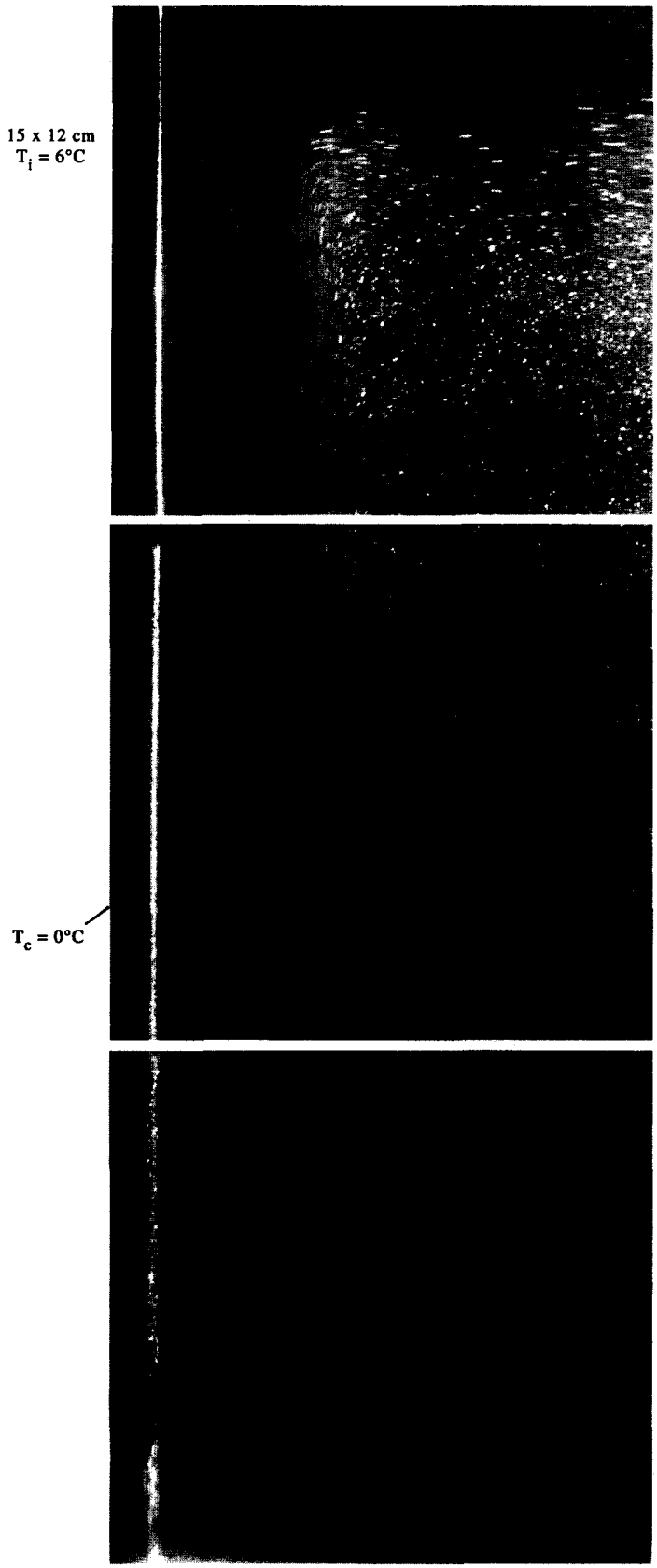

Fig. 10. Visualization photograph near the cold wall for $T_i = 6°C$ at $Ra = 1.68 \times 10^7$ corresponding to a 15×12 cm enclosure.

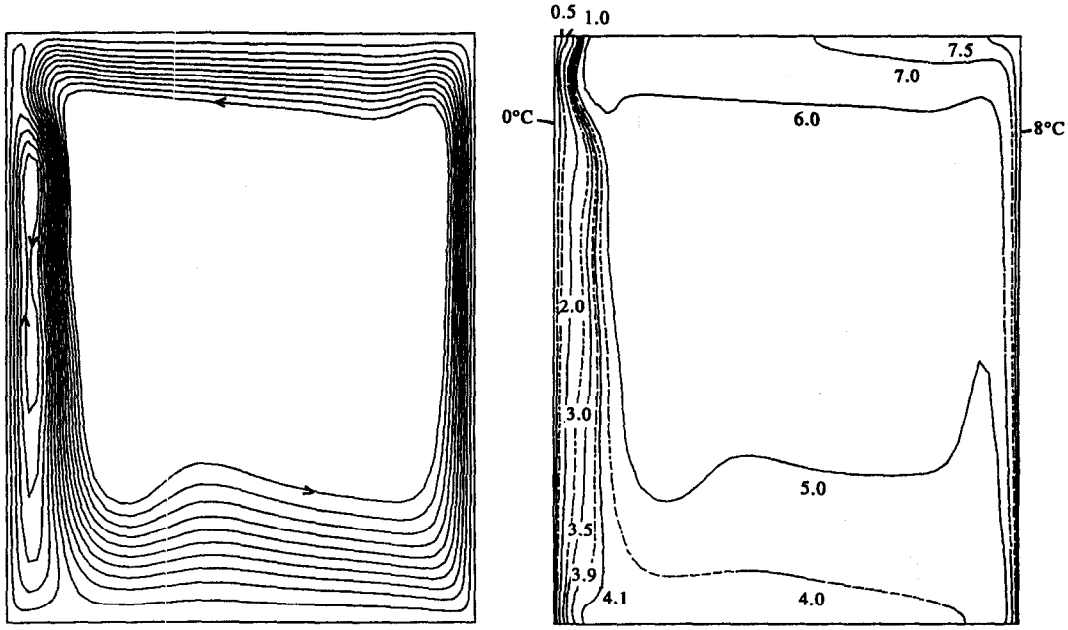

Fig. 11. Numerical steady-state streamlines and isotherms for $T_i = 6°C$ at $Ra = 1.68 \times 10^7$.

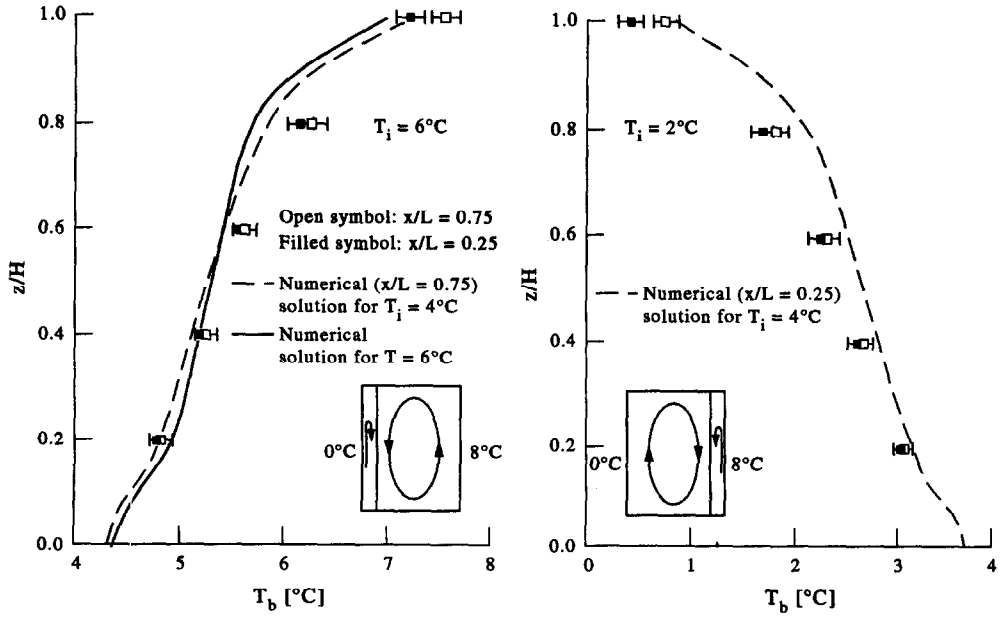

Fig. 12. Thermal stratification in the core region for $T_i = 6$ and 2°C at $Ra = 1.68 \times 10^7$.

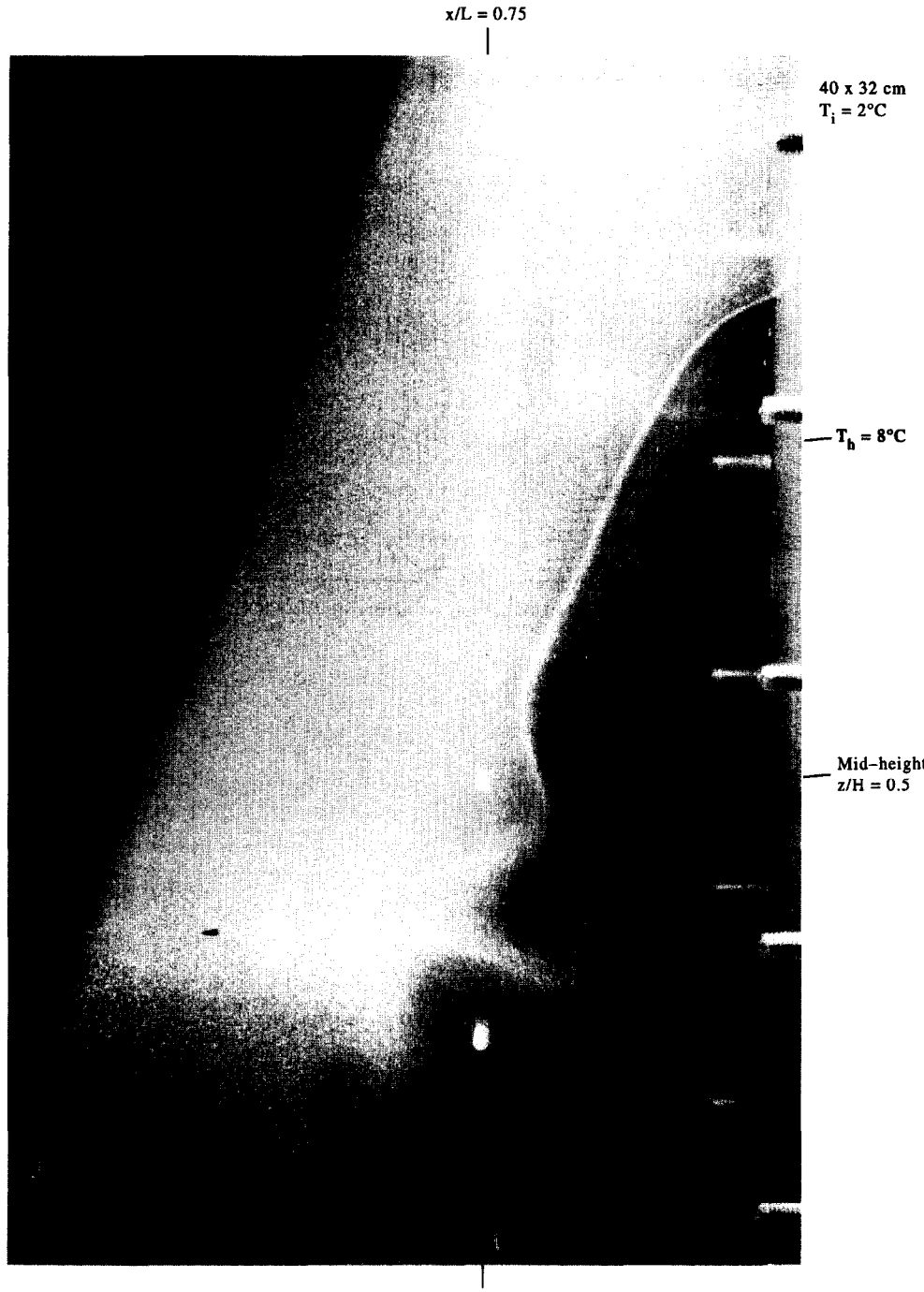

Fig. 13. Visualization photograph for $T_i = 2°C$ at $Ra = 3.2 \times 10^8$ corresponding to a 40×32 cm enclosure.

REFERENCES

1. Watson, A., The effect of the inversion temperature on the convection of water in an enclosed rectangular cavity. *Quarterly Journal of Mechanics and Applied Mathematics*, 1972, **15,** 423–446.
2. Seki, N., Fukusako, S. and Inaba, H., Free convection heat transfer with density inversion in a confined rectangular vessel. *Wärme und Stoffübertragung*, 1978, **11,** 145–156.
3. Vasseur, P. and Robillard, L., Transient natural convection heat transfer in a mass of water cooled through 4°C. *International Journal of Heat and Mass Transfer*, 1980, **23,** 1195–1205.
4. Inaba, H. and Fukuda, T., Natural convection in an inclined square cavity in regions of density inversion of water. *Journal of Fluid Mechanics*, 1984, **142,** 363–381.
5. Lin, D. S. and Nansteel, N. W., Natural convection heat transfer in a square enclosure containing water near its density maximum. *International Journal of Heat and Mass Transfer*, 1987, **30,** 2319–2329.
6. Nishimura, T., Fujiwara, M., Horie, N. and Miyashita, H., Temperature visualizations by use of liquid crystals

of unsteady natural convection during supercooling and freezing of water in an enclosure with lateral cooling. *International Journal of Heat and Mass Transfer*, 1991, **34**, 2663–2668.
7. Bennacer, R., Sun, L. Y., Toguyeni, Y., Gobin, D. and Benard, C., Structure d'ecoulement et transfert de chaleur par convection naturelle au voisinage du maximum de densite. *International Journal of Heat and Mass Transfer*, 1993, **36**, 3329–3342.
8. Tong, W. and Koster, J. N., Density inversion effect on transient natural convection in a rectangular enclosure. *International Journal of Heat and Mass Transfer*, 1994, **37**, 927–938.
9. Lankford, K. E. and Bejan, A., Natural convection in a vertical enclosure filled with water near 4°C. *Journal of Heat Transfer*, 1986, **108**, 755–763.
10. Ivey, G. N. and Hamblin, P. F., Convection near the temperture of maximum density for high Rayleigh number, low aspect ratio, rectangular cavities. *Journal of Heat Transfer*, 1989, **111**, 100–105.
11. Braga, S. L. and Viskanta, R., Transient natural convection of water near its density extremum in a rectangular cavity. *International Journal of Heat and Mass Transfer*, 1992, **35**, 861–875.
12. McDonough, M. W. and Faghri, A., Experimental and numerical analyses of the natural convection of water through its density maximum in a rectangular enclosure. *International Journal of Heat and Mass Transfer*, 1994, **37**, 783–801.
13. Nishimura, T., Wake, A. and Fukumori, E., Natural convection of water near the density extremum for a wide range of Rayleigh numbers. *Numerical Heat Transfer Part A*, 1995, **27**, 433–449.
14. Nishimura, T., Fujiwara, M. and Miyashita, H., Visualization of temperature fields and double-diffusive convection using liquid crystals in an aqueous solution crystallizing along a vertical wall. *Experimental Fluids*, 1992, **12**, 245–250.
15. Nishimura, T., Imoto, T. and Miyashita, H., Occurrence and development of double-diffusive convection during solidification of a binary system. *International Journal of Heat and Mass Transfer*, 1994, **37**, 1455–1464.
16. Simons, T. J., Circulation models of lakes and inland seas. *Canadian Bulletin of Fisheries and Aquatic Science*, 1980, **203**, 1–146.
17. Henkes, R. A. W. M., Natural convection boundary layers. Ph. D. thesis of Delft University of Technology, 1990.
18. Gogineni, S., Shih, C. and Krothapalli, Comparison of transitional free jet and wall jet. *Physical Fluid A*, 1993, **9**, S6.